Available online at www.sciencedirect.com
ScienceDirect
International Journal of Heat and Mass Transfer 50 (2007) 4493–4498
International Journal of HEAT and MASS TRANSFER
www.elsevier.com/locate/ijhmt

Technical Note

Influences of pressure gradients on freezing Poiseuille–Couette flows

Saptarshi Basu, Souma Chowdhury, Suman Chakraborty *

Department of Mechanical Engineering, Indian Institute of Technology, Kharagpur 721302, India

Received 8 September 2006; received in revised form 19 March 2007
Available online 7 June 2007

Abstract

Effects of imposed pressure gradients on the solidification characteristics of planar Poiseuille–Couette flows are mathematically investigated. Under the assumptions of quasi-steady state heat transfer, closed form expressions are obtained for the variations in the dimensionless freeze-front location and the Nusselt number, as a function of the Brinkman number, Biot number and the dimensionless pressure gradient. It is revealed that an imposed pressure gradient effectively slows down the rate of interfacial growth, irrespective of whether the pressure gradient is favourable or adverse. Non-trivial influences of the pressure gradient on the instantaneous rate of interfacial growth are also noted.

1. Introduction

Solidification in presence of Couette flow offers with a topic of immense interest for the scientists and engineers, primarily attributable to its relevance in various materials processing applications of emerging importance. For instance, one may refer to the semiconductor crystal growth processes, in which there is an interesting interplay between the parallel shear flows and directional solidification [1]. Despite such practical relevance, however, melting/solidification phase change processes in presence of Couette flows have not been extensively studied in the literature. Huang [2] were the first group of researchers to analyze the melting of semi-infinite regions in Couette flows. Analogous studies in the context of solidification heat transfer have recently been executed by Hall and Mackie [3], by addressing the problem of quasi-steady state heat transfer in a solidifying planar Couette flow with significant viscous dissipation effects. The above authors have essentially derived closed form expressions for the dimensionless freeze-front location, interface Nusselt number and the dimensionless shear stress, as functions of the pertinent non-dimensional parameters. However, the effects of pressure gradient have not been considered in their study.

Aim of the present work is to investigate the influences of imposed pressure gradients on solidification heat transfer in presence of combined pressure- and shear-driven liquid flows (Poiseuille–Couette flows). This is motivated by the consideration that in real-life material processing applications involving solidification heat transfer, a pure shear-driven flow may not be very common. In fact, in reality, pressure gradients imposed on the liquid stream, over and above the shear-driven flow actuation mechanisms, are also expected to play critical roles in the pertinent transport processes. In the present study, the regimes of numerical values for the pressure gradients and the shear rates are taken to be competitive in nature, so as to bring out an interesting and non-trivial interplay between these two mechanisms, with regard to the progress of the solid front and the overall rate of heat transfer. In particular, solutions are presented for the instantaneous locations of the solid–liquid interface and the Nusselt number, as functions of the Biot number, Brinkman number and the ratio of pressure to viscous forces.

2. Mathematical modeling

For mathematical modeling, we consider a one-dimensional region of thickness L between two parallel plates,

* Corresponding author. Tel.: +91 3222 282 990; fax: +91 3222 282 278.
E-mail address: suman@mech.iitkgp.ernet.in (S. Chakraborty).

0017-9310/$ - see front matter © 2007 Elsevier Ltd. All rights reserved.
doi:10.1016/j.ijheatmasstransfer.2007.03.037

as shown in Fig. 1. A constant axial pressure gradient (dp/dx) acts on the intervening liquid, which is initially kept at a temperature above its freezing point. The top plate moves along the horizontal direction with a constant velocity, V, whereas the bottom plate is kept stationary. The upper plate is maintained as insulated, while heat is extracted from the lower plate because of energy exchange with an ambient (the ambient being at a temperature below the freezing point of the liquid). For analyzing the problem, following major assumptions are made:

(i) The liquid is assumed to be single-component and Newtonian, with temperature-independent thermophysical properties.
(ii) The flow is considered to be laminar, fully developed and incompressible.
(iii) Axial heat conduction is neglected, in comparison to its transverse counterpart.
(iv) A quasi-steady heat transfer is assumed, as justified by the considerations of low Stefan number [4].

For mathematical modeling, the following non-dimensional parameters are employed: $Y=\frac{y}{L}$, $\Delta=\frac{\delta}{L}$, $U=\frac{u}{V}$, $\theta=\frac{(T-T_\infty)}{(T_m-T_\infty)}$, $\tau=\frac{\alpha_s t}{L^2}$, $Pr=\frac{\mu c_l}{k_l}$, $\gamma=\frac{k_l}{k_s}$, $Bi=\frac{hL}{k_s}$, $Br=\frac{\mu V^2}{k_l(T_m-T_\infty)}$, $Ste=\frac{c_s(T_m-T_\infty)}{h_{sf}}$, $C=\frac{(-dp/dx)L^2}{\mu V}$, where Y is the dimensionless transverse coordinate, Δ is the dimensionless solid-layer thickness, U is the dimensionless flow velocity, θ is the dimensionless temperature, τ is the Fourier number, Pr is the Prandtl number of the liquid, γ is the ratio of the liquid to solid thermal conductivity, Bi is the Biot number, Br is the Brinkman number, Ste is the Stefan number and C is the ratio of pressure and viscous forces.

A quasi-steady state solution of the velocity field, with the considerations made as above, can be obtained by solving the Navier Stokes equation with inconsequential transient and advective terms, as

$$U(Y,\tau)=\left[\frac{Y-\Delta(\tau)}{1-\Delta(\tau)}\right]+\frac{C}{2}(Y-\Delta)(Y-1) \tag{1}$$

The above velocity field satisfies the following boundary conditions: $U=0$ at $Y=\Delta$ and $U=1$ at $Y=1$. With this velocity variation as an input, the energy equation in the liquid phase can subsequently be solved. A non-dimensional form of this equation and the pertinent boundary conditions are as follows:

$$\frac{\partial^2\theta_l}{\partial Y^2}+Br\left(\frac{\partial U}{\partial Y}\right)^2=0 \tag{2}$$

$$\left.\frac{\partial\theta_l}{\partial Y}\right|_{Y=1}=0 \tag{3a}$$

$$\theta_l(Y=\Delta^+,\tau)=1 \tag{3b}$$

A solution to Eq. (2) can be obtained in the following form:

$$\begin{aligned}\theta_l=1&+\frac{Br}{(1-\Delta)^2}\left[\frac{1}{2}(\Delta^2-Y^2)+(Y-\Delta)\right]\\&+Br\left[\frac{C^2}{3}+\frac{C^2}{4}(\Delta+1)^2-\frac{C^2}{2}(\Delta+1)-\frac{C\Delta}{(1-\Delta)}\right](Y-\Delta)\\&-Br\left[\frac{1}{12}C^2(Y^4-\Delta^4)+\frac{C^2}{8}(\Delta+1)^2(Y^2-\Delta^2)\right.\\&-\frac{C(\Delta+1)}{2(1-\Delta)}(Y^2-\Delta^2)-\frac{C^2(\Delta+1)}{6}(Y^3-\Delta^3)\\&\left.+\frac{C}{3(1-\Delta)}(Y^3-\Delta^3)\right]\end{aligned} \tag{4}$$

For the heat diffusion in the solid, the governing equation is as follows:

$$\frac{\partial^2\theta_s}{\partial Y^2}=0 \tag{5}$$

with the appropriate boundary conditions as

$$\left.\frac{\partial\theta_s}{\partial Y}\right|_{Y=0}=Bi\,\theta_s(Y=0,\tau),\quad \tau>0 \tag{6a}$$

$$\theta_s(Y=\Delta^-,\tau)=1,\quad \tau>0 \tag{6b}$$

A quasi-steady temperature distribution can be obtained from Eq. (5) in a straight forward manner, as

$$\theta_s(Y,\tau)=\frac{Bi^{-1}+Y}{Bi^{-1}+\Delta} \tag{7}$$

The temperature distributions in the liquid and the solid phases, as represented by Eqs. (4) and (7), are coupled by the Stefan condition, as follows:

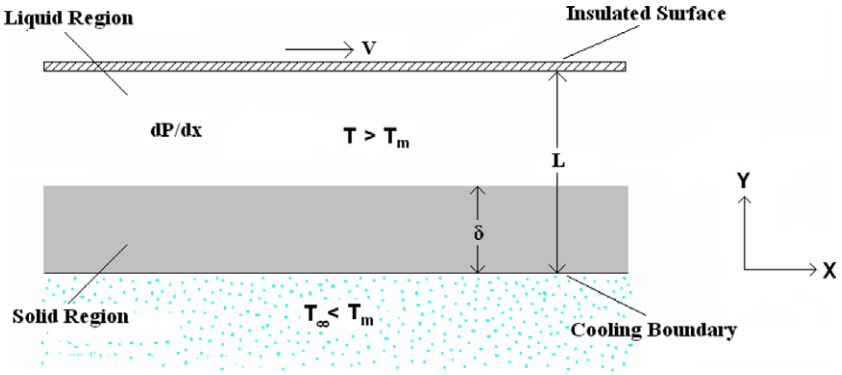

Fig. 1. A schematic diagram depicting the physical problem.

$$\left.\frac{\partial\theta_s}{\partial Y}\right|_{Y=\Delta^-} - \gamma\left.\frac{\partial\theta_L}{\partial Y}\right|_{Y=\Delta^+} = \frac{1}{Ste}\frac{d\Delta}{d\tau} \tag{8}$$

This coupling gives the temporal variation of the solid-layer thickness in the following integral form:

$$Ste\int_0^\tau d\tau = \int_0^\Delta \frac{12(1-\Delta')(Bi^{-1}+\Delta')d\Delta'}{12(1-\Delta') - \gamma Br(Bi^{-1}+\Delta')(12+C^2(1-\Delta')^4)} \tag{9}$$

The integral appearing on the right hand side of Eq. (9) can be evaluated analytically to yield the following relationship:

$$Ste\cdot\tau = c_5\cdot\sum_{i=1}^{5}\left(R_i\cdot\log\left(x + c_4R_i^4 + c_3R_i^3 + c_2R_i^2 + c_1R_i + c_0\right)\right) \tag{10}$$

where $R_i =$ Root of $(a_5R^5 + a_4R^4 + a_3R^3 + a_2R^2 + a_1R + a_0 = 0)$. In Eq. (10), c_i are numerically obtained real coefficients, based on the chosen non-dimensional parameters (namely, *Bi*, *Br* and *C*). The expressions for evaluation of a_i are as follows:

$$\begin{aligned}
a_0 &= 12 - \gamma BrC^2Bi^{-1} - 12\gamma BrBi^{-1}\\
a_1 &= -12 + 4\gamma BrC^2Bi^{-1} - \gamma BrC^2 - 12\gamma Br\\
a_2 &= -6\gamma BrC^2Bi^{-1} + 4\gamma BrC^2\\
a_3 &= 4\gamma BrC^2Bi^{-1} - 6\gamma BrC^2\\
a_4 &= -\gamma BrC^2Bi^{-1} + 4\gamma BrC^2\\
a_5 &= -\gamma BrC^2
\end{aligned} \tag{10a}$$

Finally, by utilizing the concept of the bulk mean temperature of flow, the Nusselt number is evaluated as

$$Nu = \frac{hL}{k_l} = (\theta_{l,avg} - 1)^{-1}\left.\frac{\partial\theta_l}{\partial Y}\right|_{Y=\Delta^+} \tag{11}$$

where

$$\theta_{l,avg} = \frac{T_{l,avg} - T_\infty}{T_m - T_\infty} = \frac{1}{U_m(1-\Delta)}\int_\Delta^1 U\theta_l\, dY \tag{11a}$$

In Eq. (11a), U_m is the non-dimensional average velocity, given as

$$U_m = \frac{1}{1-\Delta}\int_\Delta^1 U\, dY \tag{11b}$$

which implies

$$U_m = \tfrac{(1-\Delta)}{2} + \tfrac{C}{6}(1-\Delta^3) - \tfrac{C}{4}(1+\Delta)(1-\Delta^2) + \tfrac{C}{2}\Delta(1-\Delta) \tag{11c}$$

$$\left.\frac{\partial\theta_l}{\partial Y}\right|_{Y=\Delta^+} = Br\left(\frac{1}{(1-\Delta)} + C^2\frac{(1-\Delta)^3}{12}\right) \tag{11d}$$

$$\theta_{l,avg} = \left(\frac{1}{(1-\Delta)U_m}\right)\left(C_0(1-\Delta) + \frac{C_1}{2}(1-\Delta^2) + \frac{C_2}{3}(1-\Delta^3) + \frac{C_3}{4}(1-\Delta^4) + \frac{C_4}{5}(1-\Delta^5) + \frac{C_5}{6}(1-\Delta^6) + \frac{C_6}{7}(1-\Delta^7)\right) \tag{11e}$$

Various parameters appearing in the above expression are given in Appendix A, for the sake of completeness.

3. Results and discussion

For illustrations, the mathematical model described in Section 2 is simulated by employing different values of the significant non-dimensional numbers that effectively dictate the nature of the solidification processes, both qualitatively and quantitatively. Fig. 2a depicts the variation of the solid-layer thickness (normalized with respect to the steady state value of the same), as a function of the non-dimensional time, for different values of the parameters *C* and *Br*, with $Bi = 20$ and $\gamma = 0.5$. The nature of interfacial growth, as observed from Fig. 2a, can be explained from the consideration that as solidification progresses, the temperature gradient in the solid decreases and consequently, the heat flux in the solid side of the interface also decreases. On the other hand, a thicker solid-layer implies a thinner liquid layer through which the fluid flow may occur. In case the flow is purely shear-driven (i.e., $C = 0$), it is intuitively obvious that a thinner liquid layer would result in steeper velocity gradients in the liquid (the maximum shear velocity, namely the upper plate velocity, remaining unaltered). This, however, need not be necessarily true in case a pressure gradient acts on the flow. This is because of the fact that with a thinner liquid layer, the pressure gradient-dependent component of the flow velocity also becomes weaker in strength. The resultant velocity gradient, therefore, may increase or decrease, depending on the instantaneous thickness of the liquid layer and the pressure gradient to which the flow is subjected. During the initial transients, it is revealed that the magnitude of the velocity gradient (and hence the viscous dissipation rate) decreases monotonically with the thickening of the solidified layer. As a result, the liquid-side interfacial heat flux decreases progressively with the growth of the solid-layer. It is also observed that the difference between the solid-side and the liquid-side interfacial heat flux decreases with progress in solidification, which implies that the rate of interfacial growth also decreases. However, towards the end of the solidification process, the liquid layer becomes extremely thin and hence, the velocity gradient within the same tends to increase abruptly, leading to higher rates of irreversible conversion of mechanical energy into an equivalent intermolecular form of energy (through viscous dissipation). This augments the rate of viscous dissipation almost instantaneously, which tends to arrest the rate of interface growth considerably, towards the end of the solidification process, as evident from Fig. 2a. It can also be observed

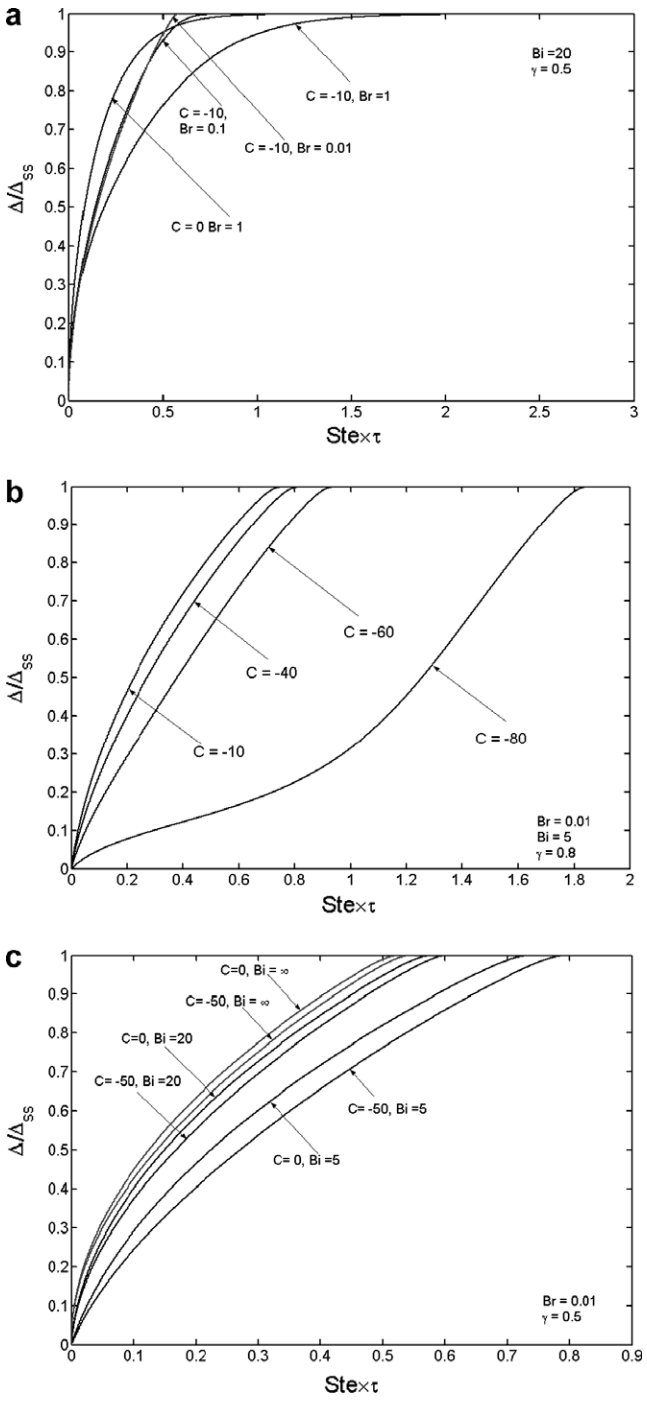

Fig. 2. Variation in the normalized freezing front location as a function of the non-dimensional time due to (a) combined variations in Br and C (b) variations in C only, and (c) variations in Bi and C.

from Fig. 2a that higher the value of Br, more retarded is the rate of interfacial growth. This can be attributed to the fact that a higher value of Br implies a greater rate of viscous dissipation and hence, a greater value of the liquid-side interfacial heat flux, thereby retarding the progress of solidification. The effect of imposed pressure gradient on the rate of interface growth, for fixed values of Br and Bi, is depicted in Fig. 2b. In plotting Fig. 2b, the value of C is only varied and the other parameters are kept unaltered ($Bi = 5$, $\gamma = 0.5$ and $Br = 0.01$). In general, it is apparent from Fig. 2b that the freezing characteristics with different magnitudes of C are qualitatively similar, with more retarded interfacial growths for higher magnitudes of C. However, on a quantitative note, there is a remarkable dissimilarity between the characteristic curves with values of C close to a critical magnitude and the values of C significantly deviated from the same. An important observation that can be made in this regard is that there can be a possibility of achieving an exact balance between the liquid and the solid side heat fluxes, in which case a further progress of solidification momentarily ceases to occur. This limiting condition can be assessed by setting the transient term in the Stefan condition to be equal to zero, which leads to the following equation:

$$\frac{1}{Bi^{-1} + \Delta_{ss}} - \gamma Br\left[\frac{1}{(1-\Delta_{ss})} + \frac{C^2}{12}(-\Delta_{ss})^3\right] = 0 \tag{12}$$

A substitution of $\Delta_{ss} = 0$ in Eq. (12) provides us with a limiting (critical) magnitude of the parameter C, beyond which physically consistent situations of interfacial growth cannot be achieved in practice. In the present situation, this limiting magnitude of the pressure gradient can be estimated as $|C_{\text{critical}}| = \sqrt{12\left(\frac{Bi}{\gamma Br} - 1\right)}$. As an illustration, for $Br = 0.01$, $Bi = 5$ and $\gamma = 0.8$, one gets $|C_{\text{critical}}| = 86.53$. Beyond this limiting magnitude of the pressure gradient, freezing is not expected to initiate at all and the solutions presented here cease to be valid. It is also interesting to observe here that for a real value of $|C_{\text{critical}}|$, one must have $Bi > \gamma Br$. There is a striking resemblance (in fact, an exact similarity) between this condition and an analogous one that has been derived in the work of Hall and Mackie [4] in the absence of any pressure gradients. With values of C close to the critical limit (such as the case with $C = -80$, as depicted in Fig. 2b), the rate of interface growth slows down considerably during the initial transients, passes through an inflexion point (with $\Delta/\Delta_{ss} \approx 0.1$), and then starts increasing again. The initial slowing down of the interfacial growth can be attributed to the progressively decreasing difference between the solid-side and the liquid-side interfacial heat fluxes at early instants of time. This difference comes to a minimum, beyond which the difference between these two heat fluxes starts increasing again. Moreover, beyond this critical juncture, a quasi-steady balance between the additional release of latent energy and an excess heating due to viscous dissipation is observed to occur, so that the time rate of relative interfacial growth becomes virtually independent of the imposed pressure gradient. As a result, the interfacial growth characteristics marked with different values of C are found to be almost parallel to each other, towards the later rapid transients. Despite this similarity in the interfacial growth characteristics, the overall freezing time is found to be considerably higher in case the value of C is taken to be close to the large limiting value, as compared to the other cases

with lower magnitudes of C, owing to the slow initial transients associated with the limiting-high pressure gradients. Fig. 2c depicts the influence of Biot number on the interfacial growth, in presence of the imposed pressure gradients. For a given value of C, a higher value of Bi tends to complete the solidification process faster, since it tends to augment the solid-side interfacial heat flux, and accordingly, to increase the difference between the solid-side and the liquid-side interfacial heat fluxes that acts as a driving potential to sustain the interfacial growth. The fastest rate of interface growth, in fact, occurs when $Bi \to \infty$, i.e., under isothermal heat extraction limits.

It is extremely important to mention here that the interfacial growth depends only on the magnitude of C and not on its sign, as evident from Eq. (9). In other words, irrespective of whether the pressure gradient is favourable or adverse, the interfacial growth characteristics are expected to be the same, provided that the magnitude of C is kept unaltered. This is because of the fact that the viscous dissipation effects depend only on the integrals of the squares of the velocity gradients, which means that the directionality effects associated with the respective pressure-driven and shear-driven components of the velocities are effectively inconsequential. This aspect can be further elucidated by referring to the typical velocity profiles corresponding adverse and favourable pressure gradients, as depicted in Fig. 3. From Fig. 3 it is evident that the velocity profiles with positive and negative values of C (with the same magnitude) turn out to be symmetric with respect to the velocity profile corresponding to $C = 0$, thereby ensuring that the viscous heat generations are independent of the sign associated with the value of C, and only the magnitude of C is consequential in this regard.

Fig. 4a depicts a representative variation of the Nusselt number (Nu) as a function of the parameters Br and C, with $Bi = 20$ and $\gamma = 0.5$ kept as unaltered. It can be observed that higher values of Br imply higher values of Nu during the initial transients. This is because of the fact that that higher values of Br are characterized with stronger viscous heating effects, which implies that augmented rates of heat extraction are necessary from the interfacial region to sustain the interface growth. This higher value of the heat flux, in turn, implies a higher value of Nu. This effect is found to be even more severe with imposed pressure gradients in the flow. For very low values of Br, on the other hand, the influence of C is rather weak, and a progressive rate of increase of the instantaneous value of Nu can be observed, provided that the magnitude of C is

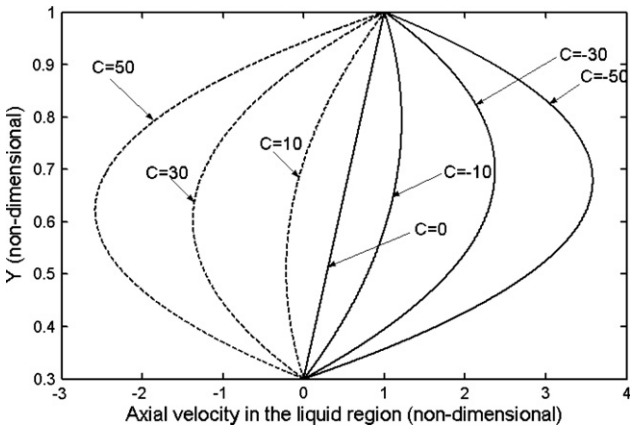

Fig. 3. Representative velocity profiles in the liquid region, for different values of C, at a time instant when the solid-layer thickness, $\Delta = 0.3$ (non-dimensional).

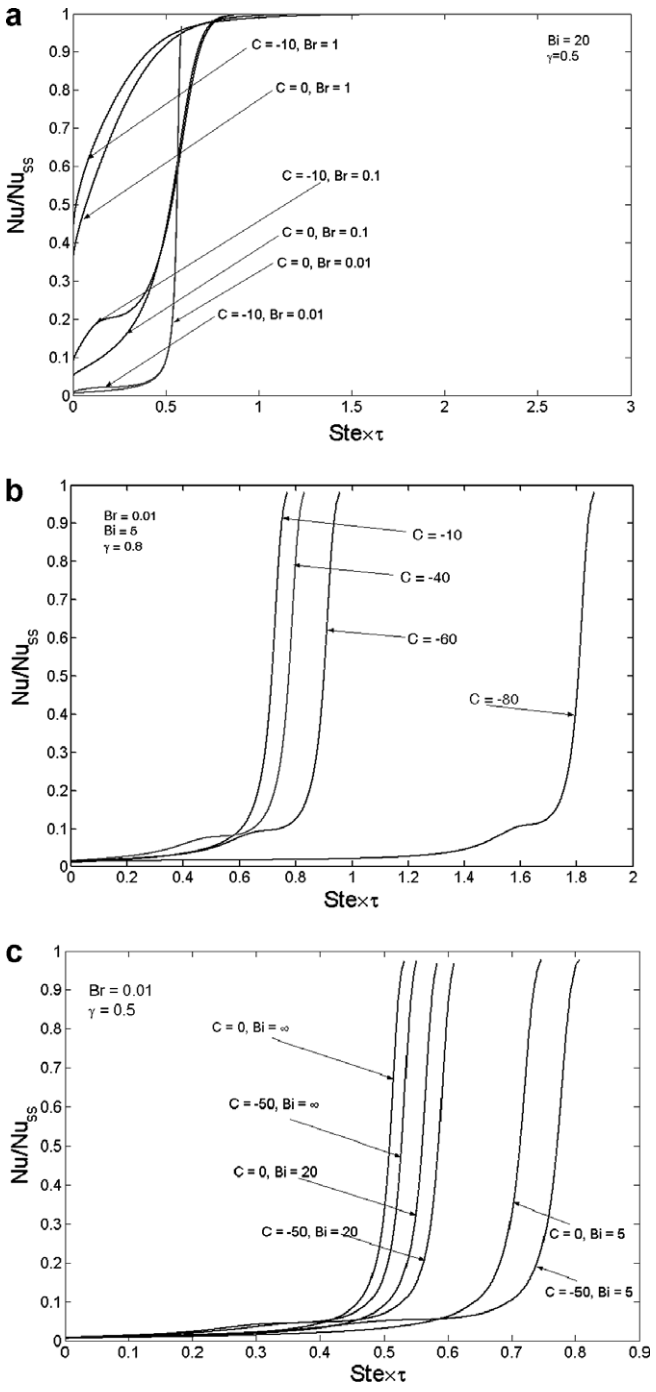

Fig. 4. Variation in the normalized Nusselt number as a function of the non-dimensional time due to (a) combined variations in Br and C (b) variations in C only, and (c) variations in Bi and C.

kept below a threshold limit. However, for higher magnitudes of C, the influence of C on Nu is quite significant, especially at lower values of $Ste \cdot \tau$, as evident from Fig. 4b. As can be seen from Fig. 4b, for the typically low value of Br (=0.01), higher magnitudes of C are characterized with significantly delayed rates of increase of Nu, before it attains its steady state value, which is quite unlike and contrasting to the cases characterized with the values of Br that are at least one order of magnitude higher than this one. This is because of the fact that for lower values of Br, the magnitude of the imposed pressure gradient dominates the overall heat transfer scenario. Further, since higher magnitudes of C essentially result in delayed interfacial growths, the initial transients associated with the variations of Nu are the slowest when the strongest pressure gradient is imposed. Towards the end of the solidification transients, the Nu increases abruptly and attains its steady state value. This is because of a sudden increment in the liquid-side interfacial heat flux towards the later transients, for reasons mentioned as earlier. Fig. 4c depicts the influence of Bi on the transients in Nu, for different values of C. As explained earlier, increases in the value of Bi imply decrements in the liquid layer thickness, and hence, result in higher rates of viscous dissipation, for the same characteristic flow velocity. On the other hand, a higher magnitude of C can result in stronger viscous heating effects (for the same liquid layer thickness), which might eventually slow down the rate of interfacial growth. As a consequence, the instantaneous Nu with a higher magnitude of C becomes somewhat less in comparison to the case with lower magnitudes of C, for the same value of Bi.

Appendix A. Details of the parameters C_0 to C_7

$$
\begin{aligned}
C_0 = {} & -\frac{\Delta}{1-\Delta}+\frac{C\Delta}{2}+\left(\frac{1}{1-\Delta}-\frac{C}{2}\right)\left[C_7-\frac{Br}{(1-\Delta)^2}\right]\Delta^2 \\
& +\left(\frac{CBr}{2}-\frac{Br}{1-\Delta}\right)\left[\frac{C^2}{12}\Delta^5+\frac{C^2}{8}(1+\Delta)^2\Delta^3\right. \\
& \left.-\frac{C(1+\Delta)}{2(1-\Delta)}\Delta^3-\frac{C^2(1+\Delta)}{6}\Delta^4+\frac{C}{3(1-\Delta)}\Delta^4\right] \\
& +\left[\frac{Br}{(1-\Delta)^3}-\frac{CBr}{2(1-\Delta)^2}\right]\left(\Delta^2-\frac{\Delta^3}{2}\right) \\
C_1 = {} & \frac{1}{(1-\Delta)}-\frac{C}{2}(1+\Delta)-\frac{2\Delta}{(1-\Delta)}\left[C_7-\frac{Br}{(1-\Delta)^2}\right] \\
& +\frac{C}{2}\Delta(\Delta+2)\left[C_7-\frac{Br}{(1-\Delta)^2}\right]-\frac{Br}{(1-\Delta)}\left[-\frac{C^2\Delta^4}{12}-\frac{C^2(1+\Delta)^2\Delta^2}{8}\right. \\
& \left.+\frac{C(1+\Delta)}{2(1-\Delta)}\Delta^2+\frac{C^2(1+\Delta)}{6}\Delta^3-\frac{C\Delta^3}{3(1-\Delta)}\right] \\
& +\frac{CBr}{2(1-\Delta)^2}\left[\left(\Delta^2-\frac{\Delta^3}{2}\right)-\left(-2\Delta+\frac{\Delta^2}{2}\right)\right]+\frac{Br}{(1-\Delta)^3}\left(-2\Delta+\frac{\Delta^2}{2}\right) \\
& -\frac{CBr}{2}\left[\frac{C^2}{12}(\Delta^5+\Delta^4)+\left(\frac{C^2}{8}(1+\Delta)^2-\frac{C(1+\Delta)}{2(1-\Delta)}\right)(\Delta^3+\Delta^2)\right. \\
& \left.+\left(\frac{C}{3(1-\Delta)}-\frac{C^2(1+\Delta)}{6}\right)(\Delta^4+\Delta^3)\right] \\
C_2 = {} & \frac{C}{2}+\left(\frac{1}{(1-\Delta)}-\frac{C}{2}(1+2\Delta)\right)\left(C_7-\frac{Br}{(1-\Delta)^2}\right) \\
& -\frac{Br}{(1-\Delta)}\left[-\frac{C^2(1+\Delta)^2\Delta}{8}+\frac{C(1+\Delta)}{2(1-\Delta)}\Delta\right] \\
& +\frac{CBr}{2(1-\Delta)^2}\left[\left(-2\Delta+\frac{\Delta^2}{2}\right)-\left(1+\frac{\Delta}{2}\right)\right]+\frac{Br}{(1-\Delta)^3}\left(1+\frac{\Delta}{2}\right) \\
& -\frac{CBr}{2}\left[-\frac{C^2\Delta^4}{12}+\frac{C^2(1+\Delta)^2\Delta(1-\Delta)}{8}-\frac{C(1+\Delta)\Delta}{2}\right. \\
& \left.+\frac{C^2(1+\Delta)\Delta^3}{6}-\frac{C\Delta^3}{3(1-\Delta)}\right] \\
C_3 = {} & \frac{C}{2}\left(C_7-\frac{Br}{(1-\Delta)^2}\right)+\frac{CBr}{2(1-\Delta)^2}\left[\frac{1}{2}+\left(1+\frac{\Delta}{2}\right)\right]-\frac{Br}{2(1-\Delta)^3} \\
& -\frac{Br}{(1-\Delta)}\left[\frac{C^2(1+\Delta)^2}{8}-\frac{C(1+\Delta)}{2(1-\Delta)}+\frac{C^2(1+\Delta)\Delta}{6}-\frac{C\Delta}{3(1-\Delta)}\right] \\
& -\frac{CBr}{2}\left[-\frac{C^2(1+\Delta)^3}{8}+\frac{C(1+\Delta)^2}{2(1-\Delta)}-\frac{C^2(1+\Delta)\Delta}{6}+\frac{C\Delta}{3(1-\Delta)}\right] \\
C_4 = {} & Br\left[\frac{C^2}{12}\frac{(2+3\Delta)}{(1-\Delta)}-\frac{7C}{12}\frac{1}{(1-\Delta)^2}-\frac{C^3}{24}\Delta-\frac{7C^3}{48}(1+\Delta)^2+\frac{5C^2}{12}\frac{(1+\Delta)}{(1-\Delta)}\right] \\
C_5 = {} & Br\left[\frac{C^3(1+\Delta)}{8}-\frac{C^2}{4(1-\Delta)}\right] \\
C_6 = {} & -Br\frac{C^3}{24} \\
C_7 = {} & Br\left[\frac{C^2}{3}+\frac{C^2}{4}(1+\Delta)^2+\frac{1}{(1-\Delta)^2}-\frac{C^2}{2}(1+\Delta)-\frac{C\Delta}{(1-\Delta)}\right]
\end{aligned}
$$

References

[1] T. Huang, S. Liu, Y. Yang, D. Lu, Y. Zhou, Coupling of couette flow and crystal morphologies in directional freezing, J. Crystal Growth 128 (1993) 167–172.

[2] S.C. Huang, Melting of semi-infinite region with viscous heating, Int. J. Heat Mass Transfer 27 (1984) 1337–1343.

[3] C.A. Hall, C. Mackie, A quasi steady analytical solution to freezing planar couette flow with viscous dissipation, J. Heat Transfer 123 (2001) 407–411.

[4] V. Alexiades, A.D. Solomon, Mathematical Modeling of Melting and Freezing Processes, Hemisphere, Washington, DC, 1993.